

First detection of the Warm Ionised Medium dust emission. Implication for the Cosmic Far-Infrared Background

G. Lagache¹, A. Abergel¹, F. Boulanger¹, F.X. Désert², and J.-L. Puget¹

¹ Institut d'Astrophysique Spatiale, Bât. 121, Université Paris XI, F-91405 Orsay Cedex

² Laboratoire d'Astrophysique, Observatoire de Grenoble, BP 53, 414 rue de la piscine, F-38041 Grenoble Cedex 9

Received 15 July 1998, Accepted 29 september 1998

Abstract. We present a new analysis of the far-IR emission at high Galactic latitude based on COBE and HI data. A decomposition of the Far-IR emission over the HI, H⁺ and H₂ Galactic gas components and the Cosmic Far InfraRed Background (CFIRB) is described.

For the first time the far-IR emission of dust associated with the Warm Ionised Medium (WIM) is evidenced. This component determined on about 25% of the sky is detected at a 10σ level in the $[200, 350] \mu\text{m}$ band. The best representation of the WIM dust spectrum is obtained for a temperature of 29.1 K and an emissivity law $\tau/N_H^+ = 3.8 \pm 0.8 \cdot 10^{-26} (\lambda/250 \mu\text{m})^{-1} \text{ cm}^2$. With a spectral index equal to 2, the emissivity law becomes $\tau/N_H^+ = 1.0 \pm 0.2 \cdot 10^{-25} (\lambda/250 \mu\text{m})^{-2} \text{ cm}^2$, with a temperature of 20 K, which is significantly higher than the temperature of dust associated with HI gas. The variation in the dust spectrum from the HI to the WIM component can be explained by only changing the upper cutoff of the Big Grain size distribution from 0.1 μm to 30 nm. The detection of IR emission of dust in the WIM significantly decreases the intensity of the CFIRB, especially around 200 μm which corresponds to the peak of energy.

the ISM far InfraRed (far-IR) emission.

Boulanger et al. (1996) have extensively studied the emission of the dust associated with the HI component using the spatial correlation between the far-IR dust emission as measured by DIRBE and FIRAS and the 21 cm HI emission as measured by the Leiden/Dwingeloo survey of the northern hemisphere. The dust emission spectrum derived from this correlation (for $N_{HI} < 4.5 \cdot 10^{20} \text{ cm}^{-2}$) can be quite well represented by a single modified Planck curve characterized by $T=17.5 \text{ K}$ and $\tau/N_{HI} = 10^{-25} (\lambda/250 \mu\text{m})^{-2} \text{ cm}^2$. This emissivity law is very close to the one predicted by the Draine & Lee (1984) dust model.

Dust emission associated with molecular clouds has been recently studied through Far-IR and submillimeter (submm) observations with the DIRBE, FIRAS and SPM/PRONAOS instruments. In a previous paper (Lagache et al., 1998), we have extensively studied the spatial distribution of the temperature of the dust at thermal equilibrium using the DIRBE and FIRAS experiment. We have found at large angular scale the presence of a cold dust component (with a median temperature of 15 K), very well correlated with molecular complexes with low star forming activity such as Taurus. The lowest values of the temperature found in the cold regions ($\sim 13 \text{ K}$) are comparable with that obtained for dense clouds in star forming regions by the balloon-borne experiment SPM/PRONAOS (Ristorcelli et al., 1996, 1998, Serra et al., 1997). The association between the cold dust component and molecular clouds is further demonstrated by the fact that all sky pixels with significant cold emission have an excess IR emission with respect to the high latitude IR/HI correlation. A threshold value of the column density, $N_{HI}=2.5 \cdot 10^{20} \text{ H cm}^{-2}$, below which cold dust is not detected within the FIRAS beam of $\sim 7^\circ$ has been deduced. This knowledge on the spatial distribution of the dust associated with cold molecular clouds is important

1. Introduction

The extraction of the Cosmic Far Infrared Background (CFIRB), induced by the emission of light from distant galaxies (Partridge & Peebles, 1967; Bond et al., 1986 and references therein), requires an accurate subtraction of the Interstellar Medium (ISM) foreground emissions. The two instruments DIRBE and FIRAS on board the COBE satellite provide actually the best available data to study, on the whole sky, the distribution and properties of

Send offprint requests to: G. Lagache

for the search of the CFIRB since it allows to select parts of the sky for which cold dust is not detected.

On the other hand, the knowledge of the dust emission associated with the H^+ component is very poor. Observations of H_α emission at high Galactic latitudes and of dispersion measures in the direction of pulsars at high $|z|$ indicate that the low-density ionised gas (the Warm Interstellar Medium, WIM) accounts for some 30% of the gas in the solar neighborhood (Reynolds, 1989). There is also evidence that part of the WIM is spatially correlated with the HI gas (Reynolds et al., 1995). Consequently, a significant fraction of the Far-IR emission associated with the WIM may contribute to the spectrum of the dust associated with the HI gas. However, the scale height of the H^+ medium is much larger than the HI one, so a significant part of the H^+ is completely uncorrelated with the HI. Since most of the grain destruction is expected to occur in the low-density component of the ISM (Mc Kee 1989), the WIM could also be dust poor. Depletion studies of elements that form the grains show that grains are indeed partly destroyed in the low density phases of the ISM (review by Savage & Sembach, 1996). Measuring the dust emission from the WIM could allow to understand the evolution of the dust in the low-density gas. However, this measure is difficult because one can not easily separate the contribution of the H^+ gas from that of the HI. Boulanger & Perault (1988) unsuccessfully searched in the 100 μm IRAS all-sky map for such a contribution. The unfruitful analysis may be due to the spatial correlation between the HI and H^+ emissions. Boulanger et al. (1996) have searched for such a component in the residual FIRAS emission after the removal of the HI component. They found that the residual emission is consistent with an emission spectrum like that of the HI gas for $N_{HI} \sim 4 \cdot 10^{19} \text{ cm}^{-2}$. However, they consider this as an upper limit for the contribution of the H^+ component since they could have measured emission from low contrasted molecular clouds. Arendt et al. (1998) have also investigated potential IR WIM dust emission. They conclude that they were unable to detect any IR emission associated with low density ionised gas at high Galactic latitude (the fraction of the sky used is less than 0.3%). However, very recently, Howk & Savage (1999) have pointed out, for the first time, the existence of Al- and Fe-bearing dust grains towards two high- z stars. They have shown that the degree of grain destruction in the ionised medium, through these two stars, is not much higher than in the warm neutral medium. If dust is present in the WIM, one should detect its infrared emission.

The CFIRB is expected to have two components: direct starlight redshifted in the far-IR and submm, and the stellar radiation absorbed by dust. We concentrate here on the submm part of this background. Its detection is very difficult because of the strong and fluctuating Galac-

tic foregrounds. First, upper limits have been reported: Hauser et al. (1995) from DIRBE data and Mather et al. (1994) from FIRAS data. Lower limits on the CFIRB have been obtained from the deepest IRAS and K galaxy counts (Hauser et al., 1994 and references therein). The first direct detection of the CFIRB has been reported by Puget et al. (1996). All the Galactic foregrounds were modeled and removed using independent dataset in addition to the FIRAS data. Its spectrum indicates the presence of sources at large redshift. The main uncertainty on the CFIRB comes from Galactic foregrounds. Therefore, we stress that the Puget et al. (1996) results were confirmed in the cleanest parts ($N_{HI} < 10^{20} \text{ cm}^{-2}$ in a 7° beam) of the sky (Guiderdoni et al., 1997). More recently, Fixsen et al. (1998) and Hauser et al. (1998) have also confirmed the detection of the CFIRB using FIRAS and DIRBE data.

A general problem with all these determinations of the CFIRB comes from a potential Far-IR emission from the WIM which has never been determined. The goal of this paper is to push our knowledge of the Galactic emission one step forward by deriving the far-IR spectrum of the WIM dust emission. Then, we use our understanding of the interstellar dust emissions associated with the HI and H^+ components to give a more accurate estimate of the CFIRB spectrum. The paper is organised as follow: in Sect. 2, we present the data we have used. The variations of the dust emission spectrum associated with different HI gas column densities are studied in Sect. 3. In Sect. 4, we show that the spatial variations of the dust emission spectrum in the low HI column density regions can be due to the presence of the non-correlated H^+ component. After the removal of the dust HI component, we detect a residual Galactic emission which is attributed to the WIM (Sect. 5). This is the first detection of the WIM dust emission. We show (Sect. 6.1) that the FIRAS spectra in the very low HI column density regions exhibit a large excess over the emission of dust associated with HI and H^+ components. In these regions, the CFIRB dominates the FIRAS emission. We test its isotropy in Sect. 6.2. All the results are summarised in Sect. 7.

2. Data presentation and preparation

The FIRAS instrument is a polarising Michelson interferometer with 7° resolution and two separate bands which have a fixed spectral resolution of 0.57 cm^{-1} (Fixsen et al. 1994). The low frequency band (2.2 to 20 cm^{-1}) was designed to study the CMB (Cosmic Microwave Background) and the high frequency band (20 to 96 cm^{-1}) to measure the dust emission spectrum in the Galaxy. We use the so-called LLSS (Left Low Short Slow) and RHSS (Right High Short Slow) data from the "pass 3" release which cover the low and high frequency bands respectively (see the FIRAS explanatory supplement). DIRBE is a photometer with ten bands covering the range

from 1.25 to 240 μm with 40 arcmin resolution (Silverberg et al. 1993). We choose to use annual averaged maps because they have a higher signal to noise ratio than maps interpolated at the solar elongation of 90° (see the DIRBE explanatory supplement). In our analysis, we only use the 140 and 240 μm maps. The present study is based on "pass 2" data.

Since in our analysis we combine the FIRAS and DIRBE data at 140 and 240 μm , we convolve the DIRBE maps with the FIRAS Point Spread Function (PSF). The PSF is not precisely known for all wavelengths, so we use the approximation suggested by Mather (private communication) of a 7° diameter circle convolved with a line of 3° length perpendicular to the ecliptic plane (Mather et al. 1986).

Before studying the Far-IR emission, we have subtracted the CMB and its dipole emission from the FIRAS data using the parameters given by Mather et al. (1994) and Fixsen et al. (1994). To remove the InterPlanetary (IP) dust emission, we first consider the 25 μm map as a spatial template for the IP dust. Then, we compute the IP dust emission at 100 μm using the zodiacal emission ratio given by Boulanger et al. (1996): $I_\nu(100)/I_\nu(25) = 0.167$. We remove the IP dust emission at $\lambda \geq 140 \mu\text{m}$ using the IP emission template at 100 μm and considering a zodiacal spectrum $I_\nu \propto \nu^3$ (Reach et al., 1995).

The HI data we used are those of the Leiden/Dwingeloo survey, which covers the entire sky down to $\delta = -30^\circ$ with a grid spacing of $30'$ in both l and b (Hartmann & Burton, 1997). The $36'$ Half Power Beam Width (HPBW) of the Dwingeloo 25-m telescope provides 21-cm maps at an angular resolution which closely matches that of the DIRBE maps. These data represent an improvement over earlier large scale surveys by an order of magnitude or more in at least one of the principal parameters of sensitivity, spatial coverage, or spectral resolution. Details of the observational and correction procedures are given by Hartmann (1994) and by Hartmann & Burton (1997). The 21cm-HI data are convolved with the FIRAS PSF. We derive the HI column densities with $1 \text{ K km s}^{-1} = 1.82 \cdot 10^{18} \text{ H cm}^{-2}$ (optically thin emission).

Throughout this paper, diffuse parts of the sky are selected following Lagache et al. (1998). To remove molecular clouds and HII regions, we use the DIRBE map of the 240 μm excess with respect to the 60 μm emission: $\Delta S = S_\nu(240) - C \times S_\nu(60)$ with $C = 4 \pm 0.7$. This map shows as positive flux regions, the cold component of the dust emission, and as negative flux regions, regions where the dust is locally heated by nearby stars (like the HII regions). Therefore, diffuse emission pixels are selected with $|\Delta S| < x\sigma$, σ being evaluated from the width of the histogram of ΔS and x being chosen for our different purposes. For example, in Sect. 5, we take $x = 1$, which is very restrictive, to ensure that the selected pixels are

mostly coming from the diffuse medium; in Sect. 6.2, we take $x = 3$, since we need a fraction of the sky as large as possible.

We also use the 240 μm /HI map excess of Reach et al. (1998). Regions for which this excess is greater than 3σ are systematically discarded.

From Lagache et al. (1998), we have for each line of sight the spectrum of the cold component of the dust emission (if cold dust is detected) and the cirrus spectrum. These spectra are used to compute the contribution of the cold dust emission in Sect. 3 (Table 1).

3. Emission spectrum of dust associated with HI gas

In this part, we first concentrate on the spatial variations of the dust emission spectrum with the HI gas column densities. We deduce a column density threshold above which the contribution of the cold dust component induces a significant submm excess with respect to the ν^2 emissivity law. Then, we investigate the spectrum of the dust associated with regions containing HI column densities below this threshold.

3.1. Variation of the dust emission spectrum with the HI column densities

To compute the emission spectrum of dust associated with HI gas from low to large column densities, we use the same method as in Boulanger et al. (1996). We first select sky pixels according to their HI column density and sort them into 10 sets of pixels bracketed by the following values of N_{HI} : [1.1, 2.7, 3.7, 4.6, 5.5, 7.3, 9.1, 10.9, 12.7, 16.4, 20.1] $\times 10^{20} \text{ H cm}^{-2}$ which correspond to W_{HI} : [60, 150, 200, 250, 400, 500, 600, 700, 900, 1100] K km s^{-1} . These different sets cover between 1.2% (for the highest column density) and 16% (for the lowest) of the sky.

Dust emission spectra are computed for each set k using the equation:

$$\frac{dF}{dN_{HI}}(k, l) = \frac{\langle F \rangle_k - \langle F \rangle_l}{\langle N_{HI} \rangle_k - \langle N_{HI} \rangle_l} \quad (1)$$

where $\langle F \rangle_i$ corresponds to the mean FIRAS spectra computed for the set of pixels i , and $\langle N_{HI} \rangle_i$ the mean HI column density for the same set of pixels. Forming the difference in Eq. 1 removes, within statistical variance, any residual IR emission which is not correlated with the HI gas such as an isotropic component.

In this part, $\langle F \rangle_k$ correspond to the FIRAS spectra computed for the 10 sets of pixels given above and $\langle F \rangle_l$ to the spectrum derived in the very low HI column density regions, $N_{HI} \leq 1.1 \cdot 10^{20} \text{ H cm}^{-2}$ (representing $\sim 2\%$ of the sky).

Table 1. Mean N_{HI} computed for different sets of pixels (see Sect.3.1). Optical depths (τ) and temperatures (T) of the HI dust emission spectra (derived following Eq. 1). Residual flux integrated in the [609-981] μm band are obtained by removing a single component ν^2 modified Planck curve (defined by τ and T) from each HI dust spectrum. The fifth column gives the percentage, in flux in the [609-981] μm band, of the detected cold emission with respect to the cirrus emission for the corresponding set of pixels (see Lagache et al., 1998 for more details).

Mean N_{HI} (H cm^{-2})	$10^{-6} \times \tau$ (normalized at 250 μm)	T (K)	Residual flux ($10^{-10} \text{ W m}^{-2} \text{ sr}^{-1}$) for $N_{HI} = 10^{20} \text{ H cm}^{-2}$	% of detected cold emission
$1.8 \cdot 10^{20}$	6.8 ± 1.8	18.0 ± 1.2	-1.0 ± 8.6	0.0
$3.2 \cdot 10^{20}$	9.8 ± 1.4	17.3 ± 0.6	3.0 ± 3.7	0.0
$4.1 \cdot 10^{20}$	9.7 ± 1.1	17.7 ± 0.5	4.0 ± 2.7	0.9
$5.0 \cdot 10^{20}$	10.2 ± 1.0	17.6 ± 0.4	4.4 ± 2.2	0.6
$6.3 \cdot 10^{20}$	11.3 ± 0.9	17.5 ± 0.3	6.4 ± 1.6	3.4
$8.1 \cdot 10^{20}$	12.1 ± 0.8	17.8 ± 0.3	9.5 ± 1.3	6.6
$9.9 \cdot 10^{20}$	13.4 ± 0.7	17.9 ± 0.2	10.9 ± 1.1	7.1
$1.2 \cdot 10^{21}$	17.1 ± 0.6	18.0 ± 0.2	13.1 ± 1.0	11.9
$1.4 \cdot 10^{21}$	16.3 ± 0.6	18.0 ± 0.2	13.9 ± 0.8	12.3
$1.8 \cdot 10^{21}$	17.1 ± 0.6	17.6 ± 0.2	13.9 ± 0.7	8.0

For each set of pixels k , the dust spectrum $\frac{dF}{dN_{HI}}(k)$ is fitted by a modified Planck curve:

$$\nu I_\nu = \tau \left(\frac{\lambda}{250 \mu\text{m}} \right)^{-2} B_\nu(T),$$

where τ is the optical depth at 250 μm , $B_\nu(T)$ is the Planck curve (in $\text{W/m}^2/\text{sr}$) and λ the wavelength in μm . The $\alpha=2$ emissivity index corresponds to standard interstellar grains (Draine & Lee, 1984). The mean temperature is equal to 17.7 K with no significant variations from set to set (Table 1, column 3). The optical depth (τ) increases linearly with the HI column density up to $N_{HI}=10^{21} \text{ H cm}^{-2}$. Then, it levels off at $\sim 1.7 \cdot 10^{-5}$ (Table 1, column 2).

We compute the residual spectrum for each set:

$$\nu R_\nu = \frac{dF}{dN_{HI}} - \nu I_\nu,$$

and study it by integrating νR_ν in the [609-981] μm band. Results are presented column 4 of Table 1 and Fig. 1. For N_{HI} larger than $5 \cdot 10^{20} \text{ H cm}^{-2}$, we detect a significant residual emission ($> 3\sigma$). Spectra at high column density contain a positive submm excess with respect to a single temperature ν^2 emissivity law Planck curve for $\lambda > 600 \mu\text{m}$. In Lagache et al. (1998), we have shown, using DIRBE data (at the FIRAS resolution), that cold emission from interstellar dust associated with H_2 gas is only detected where HI column densities are larger than $\sim 2.5 \cdot 10^{20} \text{ H cm}^{-2}$. In the Galaxy, at $|b| > 10^\circ$, 90% of this cold emission is distributed over regions with HI column densities larger than $5 \cdot 10^{20} \text{ H cm}^{-2}$. Column 5 of Table 1 gives the percentage, in flux in the [609-981] μm band, of detected cold emission for the different sets, derived from the analysis of Lagache et al. (1998). We clearly see that the submm excess increases with the contribution of the cold emission. Therefore, we conclude that this positive excess is due to the emission of cold Galac-

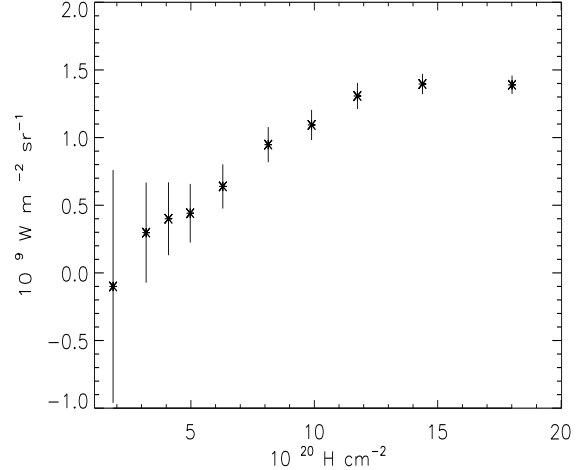


Fig. 1. Residual flux integrated in the [609-981] μm band after removing a single component modified Planck curve with $\alpha=2$ from dust spectra normalised at $N_{HI}=10^{20} \text{ H cm}^{-2}$ and computed for different HI column densities.

tic dust ($T \sim 15 \text{ K}$). We can note that the residual flux as well as the optical depth become nearly constant for $N_{HI} \geq 1.2 \cdot 10^{21} \text{ H cm}^{-2}$ since the contribution of the cold emission does not increase anymore.

In conclusion, in the diffuse medium, the spectrum of the dust associated with the HI gas can be accurately represented by a modified Planck curve with a ν^2 emissivity law and a single temperature (the residual emission is around 0, see Table 1) as it was already shown by Boulanger et al. (1996). For N_{HI} larger than $5 \cdot 10^{20} \text{ H cm}^{-2}$ ($A_v \geq 0.25$),

the cold dust ($T \sim 15$ K) induces a significant submm excess with respect to the ν^2 emissivity law.

3.2. Dust emission spectrum in low HI column density regions

In order to assess the reliability of the spectrum associated with very diffuse regions, we explore now in detail, the variations of the HI spectrum in the low HI column density medium, where the contribution of the cold dust to the total emission is negligible ($N_{HI} \leq 4.5 \cdot 10^{20}$ H cm $^{-2}$ i.e. $W_{HI} \leq 250$ K km s $^{-1}$, see Table 1). This threshold is the same as in Boulanger et al. (1996). We construct the spectrum of dust associated with HI gas following Eq. 1, for various couples (l, k) of smaller HI sets of pixels (Table 2).

Fig. 2a shows that the spectral shape of the four spectra is relatively constant but the absolute level varies by a factor ~ 1.6 between the two extremes. The two spectra obtained in regions where $N_{HI} < 2.5 \cdot 10^{20}$ H cm $^{-2}$ ($W_{HI} < 140$ K km s $^{-1}$) show a significant variation of about 30%. This variation cannot be explained by the contribution of the cold dust since (1) it is not detected in these very low HI column density regions (Table 2) and (2) the residual emission (νR_ν , see Sect. 3.1 for the definition) is around zero. Moreover, cold dust would produce an excess at long wavelength rather than a constant variation on the whole spectra. In the next section, we show some evidence that these variations of the diffuse medium spectra can be due to dust associated with the ionised gas, more specifically from small scale structures in the WIM uncorrelated with the distribution of HI gas.

Table 2. HI bins for the set of pixels l and k

W_{HI} (l) K km s $^{-1}$	W_{HI} (k) K km s $^{-1}$
[0, 50]	[50, 250]
[0, 90]	[90, 140]
[0, 50]	[50, 140]
[0, 140]	[140, 250]

4. Effects induced by the diffuse ionized gas on the Far-IR/HI correlation

To simulate the potential effect of the WIM Far-IR emission on the Far-IR/HI correlation, we have first to evaluate the hydrogen column density of the WIM. The only direct determination of the WIM column density comes from

dispersion measures in the direction of high altitude pulsars, most of which located at $|b| < 10^\circ$ (Reynolds, 1989). However, these measures, which give $N_{H^+}/N_{HI} \sim 30\%$, do not necessarily apply to the local ISM. A more direct measurement of the WIM at high Galactic latitude comes from Jahoda et al. (1990). They have measured in Ursa Major the HI emission through the 21 cm line and the H_α intensity. They have obtained $N_{HI} = 0.7 \cdot 10^{20}$ H cm $^{-2}$ and $H_\alpha = 0.2$ R. The emission measure may be converted into column density assuming a certain electron temperature and density. For $T_e = 8000$ K and $n_e = 0.08$ cm $^{-3}$ (Reynolds, 1991), we find for Ursa Major the same N_{H^+}/N_{HI} ratio ($\sim 30\%$) as with dispersion measures. In the following, we thus consider that this ratio do applied to the high latitude sky. These 30% contain the correlated (N_{cH^+}) and the non-correlated (N_{ncH^+}) H $^+$ components (by correlated, we mean spatially correlated with the HI gas).

The total hydrogen column density is defined as:

$$N_H = N_{HI} + N_{cH^+} + N_{ncH^+}.$$

We neglect the contribution of the molecular hydrogen since (1) it represents less than 1% of the emission in regions where $W_{HI} < 250$ K km s $^{-1}$ i.e. $N_{HI} < 4.5 \cdot 10^{20}$ H cm $^{-2}$ (Tables 1 and 2) and (2) the fraction of H $_2$ gas is less than 1% in the very diffuse medium (Bohlin et al., 1978). The correlated H $^+$ component can be written: $N_{cH^+} = a \times N_{HI}$. Since our knowledge on the non-correlated H $^+$ component is very poor, we choose to simulate it using two assumptions:

- (1) It is distributed in the sky like the 240 μ m emission at the same longitude but opposite latitude. This assumption is arbitrary but ensures that the non-correlated WIM gas has the same scale properties and dependance with the Galactic latitude as the diffuse interstellar medium. We note that it is essential to use, for N_{ncH^+} , a map with small scale structures to ensure the non-correlation with the HI component at small scales. This map is called \tilde{I}_{240} .
- (2) The non-correlated part of the WIM has an IR emissivity per hydrogen equal to that of the HI gas, $\tau/N_{HI} = 10^{-25} (\lambda/250 \mu\text{m})^{-2}$ (Boulanger et al., 1996). Computing τ , defined as $\tilde{I}_{240}/B_{240}(T = 17.5 \text{ K})$, gives the corresponding column density.

The map obtained with assumptions (1) and (2) is written \tilde{N}_{HI} . Thus, the uncorrelated H $^+$ component is represented by: $N_{ncH^+} = b \times \tilde{N}_{HI}$. The constraint on a and b is: $a + b = 30\%$.

Dust spectra are computed following Eq. 1, using $< N_H >_{l,k}$ rather than $< N_{HI} >_{l,k}$, for the same HI sets as in the previous section (Table 2) and for different values of a and b with a step equal to 1% and the constraint $a + b = 30\%$. We quantify the dispersion between the spectra by computing the total rms of the difference between

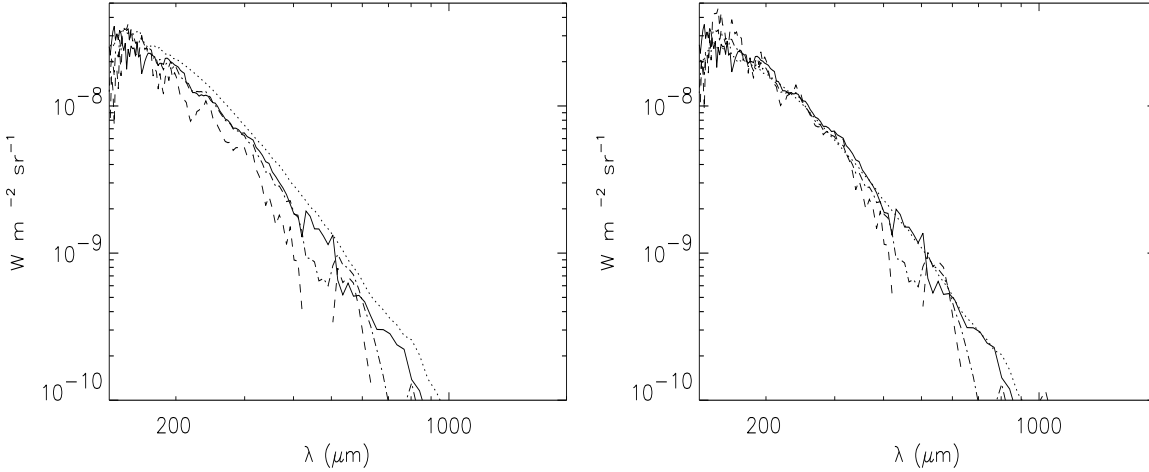


Fig. 2. (a) Spectra of dust associated with HI gas (normalised at $N_{HI}=10^{20} \text{ H cm}^{-2}$) computed following the Eq. 1 for different sets of pixels (Table 2). (b) Spectra of the dust computed in the same way as (a) and for the same sets. The normalisation is no more by HI atom but by the total hydrogen column density defined as $N_H = N_{HI} + N_{cH^+} + N_{ncH^+}$ with $N_{ncH^+} = b \times \tilde{N}_{HI}$, $N_{cH^+} = a \times N_{HI}$, $a = 0.09$ and $b = 0.21$ (see Sect. 4). The dotted line corresponds to the W_{HI} sets of pixels $[0, 140]$ and $[140, 250]$, the continuous line to $[0, 90]$ and $[90, 140]$, the dashed line to $[0, 50]$ and $[50, 140]$ and the dashed-dotted line to $[0, 50]$ and $[50, 250] \text{ K km s}^{-1}$. Spectra have been truncated below $135 \mu\text{m}$ because of the poor signal to noise ratio. They have been smoothed to a resolution of 4 cm^{-1} .

the four spectra and the mean spectrum, in the wavelength range $[200, 300] \mu\text{m}$. Fig. 2b shows the result for the minimal dispersion, obtained with $b \sim 21\%$. We see no more differences between the absolute levels of the spectra. They are all stabilized on the mean spectrum. The same conclusion is reached with other HI sets of pixel as for example: $l=[0, 50]$ and $k=[50, 190]$, $l=[0, 190]$ and $k=[190, 250]$, $l=[0, 70]$ and $k=[70, 160]$, $l=[0, 100]$ and $k=[100, 180] \text{ K km s}^{-1}$. This simulation is only illustrative but we think that it has a quantitative significance provided that the spatial distribution of the uncorrelated WIM shares the same morphological properties (ratio between small scale structures and large scale Galactic gradient) than our “DIRBE” template. This is demonstrated by the fact that the optimal b value is very stable when we rotate the H_{nc}^+ template with the Galactic longitude as long as this template stays uncorrelated with the HI component at small scales. This simulation leads to the following proportion of uncorrelated and correlated H^+ gas of 70% and 30% which are in agreement with the Reynolds et al. (1995) determination in a small region.

The emissivity of the spectrum of dust associated with the HI gas (including the H_c^+ component) that we deduce is:

$$\tau/N_{HI} = 8.7 \pm 0.9 \cdot 10^{-26} (\lambda/250 \mu\text{m})^{-2} \text{ cm}^2 \quad (2)$$

with a temperature of 17.5 K.

This emissivity value is compatible with the one derived in Boulanger et al. (1996).

5. Emission spectrum of the diffuse H^+ component

5.1. Detection

The IR emission from any dust associated with the WIM would follow a $csc(b)$ variation, like that from any diffuse component in the Galactic disk. Based on such an hypothesis, Boulanger et al. (1996) have found in the FIRAS data a residual Galactic emission (after the removal of the HI component) consistent with an emission spectrum like that of the HI gas for $N_{HI} \sim 4 \cdot 10^{19} \text{ H cm}^{-2}$. They consider this as an upper limit for the contribution of the H^+ component since they could have measured emission from low contrasted molecular clouds.

To search for any residual diffuse component after the removal of the HI contribution, we use all sky FIRAS maps at $|b| > 20^\circ$. We keep only pixels for which $|\Delta S| < 1 \sigma$ (see Sect. 2). This criterium is over restrictive (we keep only 25.6% of the sky) but ensure that the remaining pixels are mostly coming from the diffuse medium.

For each selected FIRAS spectrum $F_\nu(i, j)$, we remove the HI related emission following the equation:

$$\Delta F_\nu(i, j) = F_\nu(i, j) - N_{HI}(i, j) \times I_{HI}(\nu) \quad (3)$$

where N_{HI} the HI column density and $I_{HI}(\nu)$ is computed from $\nu I_{HI}(\nu) = \tau/N_{HI} \times B_\nu(17.5\text{K})$ where τ/N_{HI} is the HI dust emissivity given Eq. 2 and $B_\nu(17.5\text{K})$ the Planck curve at 17.5 K in $\text{W m}^{-2} \text{ sr}^{-1}$.

We first search for any residual emission by correlating the Galactic latitude emission profiles of ΔF_ν at each FIRAS wavelength, with the mean latitude emission profile computed in the wavelength range [200-350] μm . This correlation method is probably more accurate because it avoids the problems with the cosecant method linked to the local bubble. The spectrum obtained with these correlations is presented on Fig. 3. This emission is clearly non zero and is detected at a 10σ level in the [200-350] μm band. The spectrum can be fitted by a modified Planck curve with a ν^α emissivity law. The best fit is obtained for $\alpha=1$ and $T=29.1$ K. The value $\alpha=2$ is also compatible with the data. In that case, we have $T=20.0$ K, which is significantly higher than the temperature of dust associated with HI gas.

To check the Galactic origin of this residual emission, we fit the latitude profiles computed over the selected regions and for each FIRAS wavelength with cosecant variations:

$$\Delta F_\nu(|b|) \propto D_\nu \text{cosec}|b| \quad (4)$$

The slopes D_ν measured at each wavelength form a spectrum which has the same temperature and shape as the spectrum obtained with the correlation (Fig. 3). Therefore, we conclude that the spectrum derived with the correlation has a Galactic origin.

The ISM is known to contain structures over a very wide range of scales with inhomogeneous physical conditions. Within the large FIRAS beam (7°), small scale molecular clouds or HII regions can be diluted and thus not detectable using our criteria. In order to check whether such small scale structures contaminate the residual spectrum of Fig. 3, we use the same two methods (correlation and cosecant variations) to derive the spectrum using different cuts for the selection of the pixels (either more or less restrictive than above). The spectra obtained with correlations or cosecant laws are very stable. This supports the idea that the residual Galactic emission cannot be due to low contrasted molecular clouds or HII regions. Moreover, to check whether this residual Galactic emission is not dominated by a particular region of the sky, we repeat the same cosecant fit analysis in 4 bins of longitude of roughly equal size (6% of the sky each). The small number of pixels does not allow to have a better sampling. We see, in Table 3, that the residual Galactic component is present in the 4 different bins with small variations. Therefore, we can exclude this residual Galactic component to come from a particular region of the sky.

The residual Galactic spectrum corresponds to material which is uncorrelated with the HI gas (by construction). However, it is Galactic because it follows a cosecant law. We propose that this is the first detection of the submm emission of dust associated with the WIM.

Table 3. Cosecant slopes (νD_ν) of the residual Galactic emission averaged in the wavelength band [200,350] μm and computed in different Galactic longitude areas.

Galactic longitude range (in $^\circ$)	Residual Galactic emission ($10^9 \text{ W m}^{-2} \text{ sr}^{-1}$)
0 - 85	9.4 ± 0.5
85 - 170	6.4 ± 0.4
170 - 235	9.9 ± 0.6
235 - 360	10.7 ± 0.7

5.2. Normalisation and emissivity

To normalise the WIM far-IR spectrum, we make use of the cosecant law measured for H_α emission at high Galactic latitude. The slope of the H_α cosecant law is equal to 1 R (Reynolds et al., 1984). This gives (following the results obtained in Sect. 4: 70% of 1R) 0.7 R for the non-correlated H^+ gas. Using a conversion factor $I_{H\alpha}(R) = 1.15 \times N_H^+/10^{20} \text{ cm}^{-2}$ (derived from Osterbrock, 1989), we obtain $N n_{CH^+} = 6.1 \times 10^{19} \text{ cm}^{-2}$. This column density is close to that derive from the pulsar observations (Reynolds, 1989).

Using this normalisation, the emissivity per H^+ ions is: $\tau/N_H^+ = 3.8 \pm 0.8 \times 10^{-26} (\lambda/250 \mu\text{m})^{-1} \text{ cm}^2$. The uncertainty corresponds to the 21 % dispersion observed in the different longitude bins (Table 3). With a ν^2 emissivity law, we find $\tau/N_{H^+} = 1.0 \pm 0.2 \times 10^{-25} (\lambda/250 \mu\text{m})^{-2} \text{ cm}^2$. This emissivity value agrees within error bars with the emissivity of dust associated with HI gas.

We have not taken into account until now of the uncertainty on the HI dust emission spectrum. The removal of the HI maximal spectrum, defined by $\tau/N_{H^+} = 9.6 \times 10^{-25} (\lambda/250 \mu\text{m})^{-2}$ (see Eq. 2) and $T=17.5$ K, only decreases the emissivity of the WIM dust component by 30%; the removal of the minimal spectrum, defined by $\tau/N_{H^+} = 7.8 \times 10^{-26} (\lambda/250 \mu\text{m})^{-2}$ and $T=17.5$ K, increases the emissivity by 24%.

The spectrum derived from the slopes of the cosecant law (which measures the Galactic emission in a direction perpendicular to the Galactic disk over a significantly large area) corresponds to the submm dust emission of an HI equivalent column density of 10^{20} cm^{-2} (this value is estimated using D_ν and $I_{HI}(\nu)$), which is higher than the tentative detection of Boulanger et al. (1996) due to the difference in the HI dust spectrum used for the normalisation. Since this column density of 10^{20} cm^{-2} is roughly the Reynolds's estimate of the total H^+ column density, our result is consistent with a dust abundance in the WIM which does not differ much from that of the HI gas. We reach the same conclusion using the minimal or maximal HI spectrum. However, this conclusion is still preliminary since the Reynolds's estimate is made in parts of

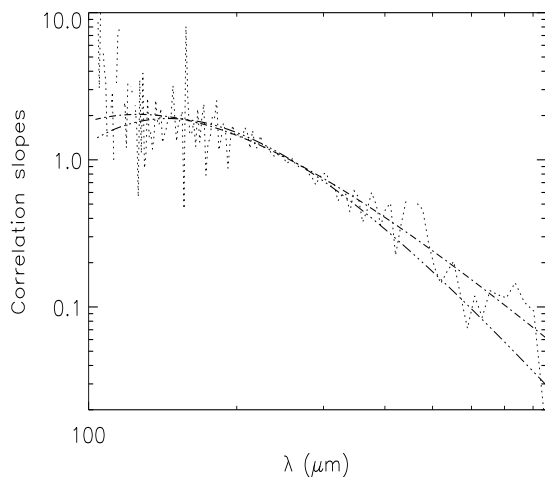


Fig. 3. Correlations slopes of the residual Galactic emission (dotted line) after the main HI component has been removed (slopes have been computed using the residual Galactic emission in I_ν). The dash-dotted line represents a modified Planck curve with $\alpha=1$, $T=29.1$ K and the dot-dot-dot-dashed line a modified Planck curve with $\alpha=2$ and $T=20$ K. This spectrum is the first detection of the WIM dust emission

the sky which are different from those used here. Future comparison of the Far-IR dust emission with the Wisconsin H-Alpha Mapper survey (WHAM, Tufté et al., 1996; Reynolds et al., 1998) will allow to give a more precise estimate on the dust abundance in the WIM.

5.3. First interpretation

It is extremely difficult to disentangle whether the WIM spectrum follows a ν^2 or a ν^1 emissivity law because of the poor signal to noise ratio of our spectrum at long wavelength (Fig. 3). However, this spectrum has a definitively higher temperature than the spectrum of dust associated with HI gas.

Dust grains in the WIM are expected to have smaller sizes due to grain shattering in grain-grain collisions (Jones et al., 1996, Fig. 17). We have used the dust model developed by Désert et al. (1990) to test the effect of the size distribution on the Far-IR spectrum. First, a standard Big Grains composition and size distribution (abundance in mass $m/m_H = 5 \cdot 10^{-3}$ ¹, silicates with dark refractory mantle composition, distribution in size following a 2.9 power law with $a_{min}=15$ nm and $a_{max}=110$ nm, and a density of 3 g/cm^3) remarkably reproduce the dust emission spectrum associated with the HI gas (Fig. 4, upward curve). A smaller cutoff in the size distribution (with

¹ This abundance in mass is lower than the one given in Désert et al., 1990 due to the difference of calibration between the IRAS and DIRBE/FIRAS instruments

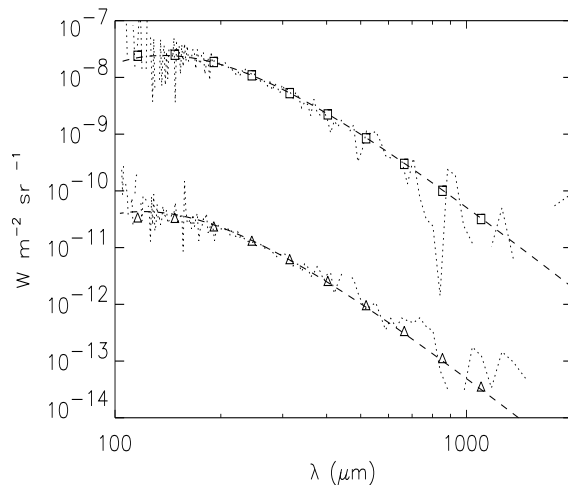


Fig. 4. Upward curves: HI dust emission spectrum (dotted line), HI synthetic spectrum (corresponding to the emissivity and temperature given in Sect. 4, dashed line) and HI emission model (square) for $N_{HI} = 10^{20} \text{ cm}^{-2}$. Downward curves: H^+ dust emission spectrum (dotted line, divided by $1.5 \cdot 10^3$), H^+ synthetic spectrum (corresponding to the emissivity and temperature given in Sect. 5, dashed line) and H^+ emission model (triangle) for $N_{H^+} = 10^{20} \text{ cm}^{-2}$.

$a_{max}=30$ nm, which is compatible with what is predicted in Jones et al., 1996) is needed to reproduce the spectrum of the WIM (Fig. 4, downward curve). This comparative analysis suggests that the difference of temperature between the HI and H^+ diffuse media can be explained by the erosion of the dust grains due to the collisions.

6. The extragalactic component

6.1. FIRAS spectra in low HI column density regions: evidence for an extragalactic component

Puget et al. (1996) have found in the residual emission after the removal of the HI correlated emission, an isotropic component which could be the Cosmic Far Infrared Background (CFIRB) due to distant Galaxies. At $|b| > 40^\circ$, at least one third of the emission at $500 \mu\text{m}$ comes from this isotropic component. Thus, at high Galactic latitude in very low HI column density regions, this component should dominate the FIRAS emission.

We have selected pixels for which $N_{HI} < 9.1 \cdot 10^{19} \text{ H cm}^{-2}$ and $b > 40^\circ$ (33 pixels). These pixels are located near and in the Lockman Hole and represent 0.54% of the sky. For this set of pixels, the mean HI column density is equal to $8 \cdot 10^{19} \text{ H cm}^{-2}$. In this region, the non-correlated H^+ column density is estimated using $N_{H^+}/N_{HI}=30\%$ (Jahoda et al., 1990) which gives $N_{H^+}/N_{HI}=21\%$ (see Sect. 4). We clearly see (Fig. 5) that the emission of dust associated with the HI and H^+ components cannot account for the FIRAS spectrum, especially at $\lambda > 300 \mu\text{m}$. The presence

of another component is evident. The level of this component is the same as the residual FIRAS emission obtained in Puget et al. (1996) before they subtract the estimated H^+ and is in very good agreement with the Fixsen et al. (1998) determinations. Puget et al. (1996) have shown that the most likely interpretation for this component is the Cosmic Far-Infrared Background (CFIRB) due to the integrated light of distant galaxies. Despite the fact that it is not physical to consider a unique temperature for this background, it can be analytically represented in the same way as in Fixsen et al. (1998). The best fit, valid between 200 and 2000 μm ,

$$I(\nu) = 8.80 \times 10^{-5} (\nu/\nu_0)^{1.4} B_\nu(13.6K) \quad (5)$$

where $\nu_0 = 100 \text{ cm}^{-1}$, is presented on Fig. 6, together with the range of determination of Fixsen et al. (1998). The uncertainties on the fit will be discussed in a forthcoming paper (Gispert et al., 1999).

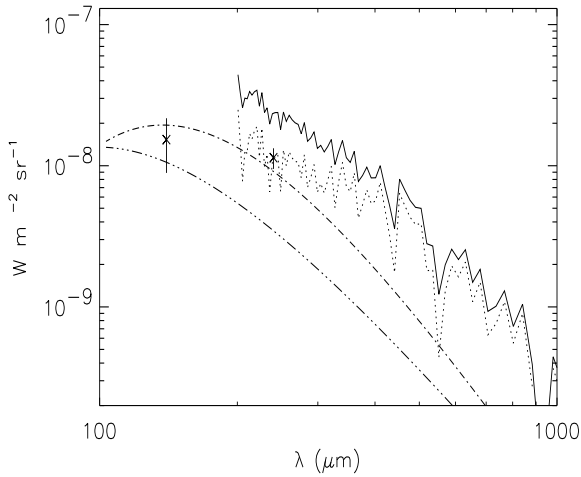


Fig. 5. Mean FIRAS (continuous line), HI (dash-dot) and H^+ (dash-dot-dot-dot) spectra in regions where $N_{HI} < 9.1 \times 10^{19} \text{ H cm}^{-2}$. The residual emission (dot line), obtained by removing from the mean FIRAS spectrum the HI and H^+ components, dominates the FIRAS emission at high latitude in low HI column density regions. The typical uncertainties for this residual emission are around $2.6 \times 10^{-9} \text{ W m}^{-2} \text{ sr}^{-1}$ for $200 < \lambda < 400 \mu\text{m}$, $1.75 \times 10^{-9} \text{ W m}^{-2} \text{ sr}^{-1}$ for $400 < \lambda < 600 \mu\text{m}$, and $2.5 \times 10^{-10} \text{ W m}^{-2} \text{ sr}^{-1}$ for $\lambda > 600 \mu\text{m}$. Also reported are our determinations of the DIRBE CFIRB at 140 and 240 μm (cross points, see Table 4).

The CFIRB can also be determined at 240 and 140 μm using DIRBE data for the same part of the sky. Results are presented in Table 4 together with previous determinations. In this Table, uncertainties on total emissions are

the dispersions measured for the selected pixels, uncertainties on the HI dust emissions are given by Eq. 2, and uncertainties on the WIM dust emissions correspond to the 21% dispersion observed in the four bins of Galactic longitude (Table 3). Our residual emissions (Res2 in Table 4) are significantly lower than the ones reported in Hauser et al. (1998) and Schlegel et al. (1997) since they have neglected the contribution of the dust associated with the WIM. We clearly see that it is essential to take into account the dust emission associated to the WIM below 240 μm . In FIRAS data at 240 μm , the CFIRB emission (Fig. 5) is very close to our DIRBE value. At 140 μm , the comparison between DIRBE and FIRAS data is not possible due to the considerable increase of the FIRAS data noise (that is why we have preferred to cut the spectrum at 200 μm in Fig. 5).

6.2. Isotropy

We test in this part the isotropy of the CFIRB on large scales since we do not know the spatial distribution of the WIM dust emission at small angular scales. This test at large scales is important to detect potential systematic effects caused by an inaccurate subtraction of ISM dust emissions. As expected from our detection of the WIM dust emission, we show that the CFIRB is isotropic only if we consider the emission of dust associated with the H^+ component.

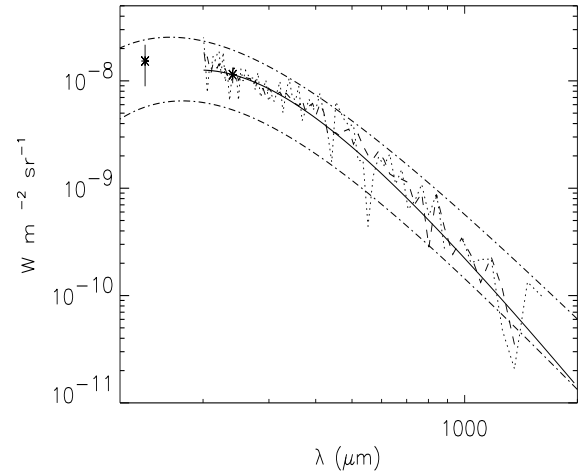


Fig. 6. CFIRB emission computed on 51% (dashed line) and on 0.54% of the sky (dotted line). The continuous and dotted-dashed lines correspond to the analytic forms of the CFIRB given by Eq. 5 and Fixsen et al. (1998) respectively. Cross points correspond to our DIRBE CFIRB values at 140 and 240 μm (Res2 of Table 4).

Table 4. Contribution of the different components to the DIRBE 140 and 240 μm emissions in the Lockman Hole region where the mean HI column density is $8 \cdot 10^{19} \text{ H cm}^{-2}$. Res2 corresponds to the CFIRB values.

Component	140 μm $10^8 \text{ W m}^{-2} \text{ sr}^{-1}$	240 μm $10^8 \text{ W m}^{-2} \text{ sr}^{-1}$
Total	4.53 ± 0.57	2.40 ± 0.15
$\text{HI} + \text{H}_c^+$	1.94 ± 0.19	0.91 ± 0.09
$\text{Res1} = \text{Total} - (\text{HI} + \text{H}_c^+)$	2.59 ± 0.60	1.49 ± 0.17
H_{nc}^+	1.06 ± 0.22	0.35 ± 0.07
$\text{Res2} = \text{Total} - (\text{HI} + \text{H}_c^+) - \text{H}_{nc}^+$	1.53 ± 0.64	1.14 ± 0.19
Residual ¹	2.50 ± 0.70	1.36 ± 0.25
Residual ²	3.19 ± 0.43	1.67 ± 0.17

¹ Hauser et al., 1998

² Schlegel et al., 1998

Thus, we have to compute the CFIRB spectrum on a fraction of the sky as large as possible. For that, we prefer to use a Galactic template based on far-IR emissions rather than HI gas, (1) to take into account variations in the dust temperature from place to place and (2) to avoid the large hole in the southern hemisphere of the Leiden/Dwingeloo survey. We combine the DIRBE 140 and 240 μm data with FIRAS spectra. First, we extract from DIRBE data (at 7° resolution) a Galactic emission template. Then, the DIRBE Galactic emission is extrapolated to longer wavelengths and subtracted from each individual selected FIRAS spectrum to derive the CFIRB emission and test its isotropy.

The two (140 and 240 μm) Galactic DIRBE templates, I_G , are computed by removing the CFIRB (Table 4) from the DIRBE emissions. Assuming a ν^2 emissivity law, temperature and optical depth of each pixel are estimated using the two DIRBE Galactic templates. The residual FIRAS emission is computed in the following way. First, we discard pixels located in known molecular clouds or HII regions. We keep pixels with $|\Delta S| < 3\sigma$ and work at $|b| > 15^\circ$ (51% of the sky). Then, for each selected pixel with its associated temperature, we derive the ratio R_ν between the modified Planck curve computed at each FIRAS wavelength and the modified Planck curve computed at 240 μm . Finally, the residual emission is computed in the following way:

$$\text{Res}_\nu(i, j) = F_\nu(i, j) - R_\nu \times I_G(i, j) \quad (6)$$

The mean residual emission spectrum is shown Fig. 6 together with the spectrum obtained on 0.54% of the sky and its analytical determination (Eq. 5). The two spectra agree very well.

The isotropy of our residual emission is addressed by looking at its variation with the Galactic longitude or latitude. The variation of our residual with the Galactic longitude is derived by computing the mean residual emission

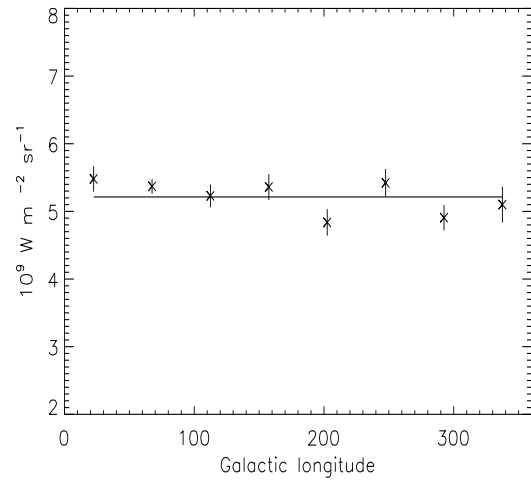


Fig. 7. Variation of the FIRAS residual emission averaged in the $[300, 609] \mu\text{m}$ band with the Galactic longitude. The error bars are statistical errors (1σ).

(in the $[300, 609] \mu\text{m}$ band) in 8 different longitude bins (each bin representing around 3.5% of the sky). The profile, shown in Fig. 7, does not show any particular Galactic structure. To test the isotropy with the Galactic latitude, we compute the emission profile versus the latitude (cosecant variation) of our residual emission (Fig. 8a). We clearly see a residual Galactic component. The slope of the fitted cosecant law is $\sim 7 \cdot 10^{-10} \text{ W m}^{-2} \text{ sr}^{-1}$ which is 4 times smaller than the slope of the H_{nc}^+ cosecant component.

The pixels selected before represent only the diffuse medium but contain both the neutral and ionised emission and thus cannot be very well represented by a sin-

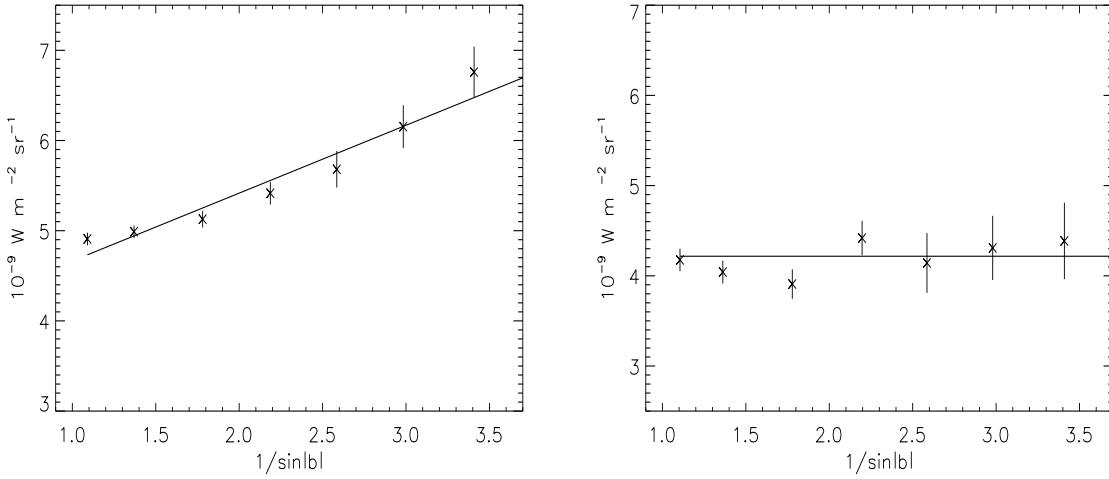


Fig. 8. a. Variation of the FIRAS residual emission averaged in the $[300, 609] \mu\text{m}$ band with the Galactic latitude. b. same as (a) but the FIRAS residual has been computed by taking into account dust emission from the WIM.

gle temperature component. Therefore, our residual FIRAS emission could be affected by an inaccurate subtraction of the interstellar medium emissions. To test the effect of the presence of the WIM dust emission on our residual emission, we apply the same method as previously but remove from the DIRBE data, before determining the temperatures, the H_{nc}^+ dust emission defined as $Enc_{H^+}(i, j, \nu) = b \times \tilde{N}_{HI}(i, j) \times Inc_{H^+}(\nu)$ with $b = 0.21$ (see Sect. 4). $Inc_{H^+}(\nu)$ represents the non-correlated H_{nc}^+ spectrum derived in Sect. 5. The FIRAS residual emission is computed in the following way:

$$Res_{\nu}(i, j) = F_{\nu}(i, j) - R'_{\nu} \times I'_G(i, j) - Enc_{H^+}(i, j, \nu) \quad (7)$$

where R'_{ν} and I'_G represent the new ratio and DIRBE $240 \mu\text{m}$ neutral Galactic template respectively, obtained after removing the contribution of the dust emission associated with the non-correlated HII component. The mean residual emission is in very good agreement with the previous estimates (Fig. 6). Moreover, we see no more residual cosecant variations (Fig. 8b): the residual component of Fig. 8a was due to the non-correlated H^+ emission.

In conclusion, we clearly show that the main uncertainty to the CFIRB determination on individual pixels of the sky comes from dust emission associated with the non-correlated H^+ component.

7. Conclusions

A new analysis of the correlation between gas and dust at high Galactic latitude has been presented. For the first time, we are able to present a decomposition of the Far-IR emission over the HI, H^+ and H_2 gas with the determination of the dust emission spectrum for each of these components. This decomposition is important to study the

evolution of interstellar dust as well as to give new constraints on the CFIRB (spectrum and test of isotropy).

The data used in this analysis are the COBE far-IR data and the Leiden-Dwingeloo HI survey. Our decomposition is based on the IR/HI correlation and DIRBE and FIRAS IR colors. The main quantitative results of this work follow:

1) Dust emission spectrum associated with the HI gas: We confirm that the emission spectrum of dust in HI gas is well fitted by a modified Planck curve with a ν^2 emissivity law and a temperature of 17.5 K. However, the emissivity normalised per H atom varies by about 30% depending on the pieces of the sky used to compute the spectrum. We show that this variation may be explained by the emission of the dust associated with the H^+ component. Taking into account this contribution, we derive a new value of the dust emissivity normalised per hydrogen atom: $\tau/N_{HI} = 8.7 \pm 0.9 \cdot 10^{-26} (\lambda/250 \mu\text{m})^{-2} \text{ cm}^2$ with a temperature of 17.5 K, slightly lower than the previous determination of Boulanger et al. (1996).

2) Dust emission spectrum associated with the H^+ gas: The existence of far-IR emission from the WIM is demonstrated by the latitude dependance of the residuals of the IR/HI correlation. This cosecant variation gives a spectrum which is clearly different from the HI dust spectrum. This component is detected at a 10σ level in the $[200-350] \mu\text{m}$ band. Dust associated with the WIM has an emissivity $\tau/N_{H^+} = 3.8 \pm 0.8 \cdot 10^{-26} (\lambda/250 \mu\text{m})^{-1} \text{ cm}^2$ with a temperature of 29.1 K. With a spectral index equal to 2, the emissivity law becomes $\tau/N_{H^+} = 1.0 \pm 0.2 \cdot 10^{-25} (\lambda/250 \mu\text{m})^{-2} \text{ cm}^2$ with a temperature of 20 K. The variation in dust spectrum from the HI to the WIM dust component can be explained by only changing the upper cutoff of the Big Grain size dis-

tribution from 0.1 μm to 30 nm.

3) Cosmic Far-IR Background (CFIRB):

FIRAS spectra in low HI column density regions (0.54% of the sky) clearly show the presence of a component which is not associated with the HI and H^+ gas and which is interpreted, following Puget et al. (1996), as the CFIRB due to the integrated light of distant galaxies. The determination of this component on 51% of the sky confirms its isotropy at large scale on a suitable fraction of the sky. With our determination of the WIM contribution to the far-IR sky emission, we find for the CFIRB values at 140 and 240 μm , $1.53 \pm 0.64 \cdot 10^{-8}$ and $1.14 \pm 0.19 \cdot 10^{-8} \text{ W m}^{-2} \text{ sr}^{-1}$ respectively, which are significantly lower than the Hauser et al. (1998) determinations. The contribution of the IR dust emission from the WIM relative to the CFIRB is negligible at longer wavelengths.

Acknowledgements. We are grateful to the Goddard Space Flight Center team for introducing us to the COBE data.

References

- Arendt, R.G. et al., 1998, ApJ 508, 74
 Bohlin, R.C. et al., 1978, ApJ 224, 132
 Bond, R.J. et al. 1986, ApJ 306, 428
 Boulanger, F., & Péroult, M. 1988, ApJ 330, 964
 Boulanger, F. et al. 1996, A&A 312, 256
 Désert, F.X., Boulanger, F., Puget, J.L. 1990, A&A 237, 215
 Draine, B.T. & Lee, H.M. 1984, ApJ 285, 89
 Fixsen, D.J. et al. 1994, ApJ 420, 457
 Fixsen, D.J. et al. 1998, ApJ 508, 123
 Gispert, R., Lagache, G. & Puget, J.L. in preparation
 Guiderdoni, B. et al., 1997, Nature 390, 257
 Hartmann, D. 1994, Ph.D. Thesis, University of Leiden
 Hartmann, D. & Burton, W.B., "Atlas of Galactic neutral Hydrogen", Cambridge University Press, 1997
 Hauser, M.G. et al., in "Examining the Big Bang and Diffuse Background Radiations, IAU symp. 168", The Hague, 1994
 Hauser, M.G. et al., in "Unveiling the Cosmic Infrared Background" ed. E. Dwek, AIP Conf. Proc., 1995
 Hauser, M.G. et al., 1998, ApJ 508, 25
 Howk, J.C. & Savage, B.D., ApJ, in press
 Jahoda, K., Lockman, F.J., McCammon, D. 1990, ApJ 354, 184
 Jones, A.P. et al., 1996, ApJ 469, 740
 Lagache, G., Abergel, A., Boulanger, F., Puget, J.L. 1998, A&A 333, 709
 Mather, J.C. et al. 1986, App Opt 25, 16
 Mather, J.C. et al. 1994, ApJ 420, 439
 McKee, C.F. 1989, in "Interstellar Dust", eds L.J. Allamandola and A.G.G.M. Tielens, p431, Kluwer
 Osterbrock, D.E., "Astrophysics of Gaseous Nebulae and Active Galactic Nuclei", University science book, 1989
 Partridge, R.B. & Peebble, P.J.E. 1967, ApJ, 148, 377
 Puget, J.L. et al. 1996, A&A 308, L5
 Reach, W.T. 1998, ApJ 507, 507
 Reach, W.T. 1995, in "Unveiling the Cosmic Infrared Background" ed. E. Dwek, AIP Conf. Proc.
 Reynolds, R.J. et al., 1984, 282, 191
 Reynolds, R.J. 1989, ApJ 339, L29
 Reynolds, R.J. 1991, ApJ 372, L17
 Reynolds, R.J. 1992, ApJ 392, L35
 Reynolds, R.J. et al., 1995, ApJ 448, 715
 Reynolds, R.J. et al., 1998, PASA 15, 14
 Ristorcelli, I., et al. 1998, to be submitted
 Ristorcelli, I. et al. 1996, in "Diffuse infrared radiation and the IRTS", Ed. H. Okuda, T. Matsumoto, T. Roelling
 Tufte, S.L., et al., 1996, BAAS, 28, 890
 Savage, B.D. & Sembach, K.R. 1996, ARAA, 34, 279
 Schlegel, D.J., Finkbeiner, D.P., Davis, M. 1998, ApJ 500, 525
 Serra, G. et al. 1997, in "The Far Infrared and Submillimetre Universe", ESA SP-401
 Silverberg, R.F. et al. 1993, in SPIE Conference Proc. 2019 on Infrared Spaceborne Remote Sensing, San Diego